Electronic Supplementary Material (ESI) for Journal of Materials Chemistry A.

# Supporting information

## Thermodynamic study at 25 °C

$$\Delta_r G^{\ominus}_{m} = \left[c\Delta_f G^{\ominus}_{m}(C) + d\Delta_f G^{\ominus}_{m}(D)\right] - \left[aG^{\ominus}_{m}(A) + b\Delta_f G^{\ominus}_{m}(B)\right]$$

$$CH_3CHOHCH_3 + \frac{1}{2}O_2 = CH_3COCH_3 + H_2O$$

$$\Delta_r G^{\ominus}_{m} = \Delta_f G^{\ominus}_{m}(CH_3COCH_3) + \Delta_f G^{\ominus}_{m}(H_2O) - \Delta_f G^{\ominus}_{m}(CH_3CHOHCH_3) - 0.5 \times \Delta_f G^{\ominus}_{m}(O_2)$$

$$\Delta_r G^{\ominus}_{m} = -152.7 + (-298.2) - (-137.4) - 0.5 \times (-61.2) = -282.9\ kJ/mol$$

$$\Delta G = -RTlnK$$

$$\Delta G = -RTln\frac{(acetone)(water)}{(2-propanol)(oxygen)^{\frac{1}{2}}}$$

In 500 mL reactor, the amounts of oxygen could be approximately calculated as 500/22.4×0.2×1000＝4460 μmol; Initial IPA is 20 μmol;

After a certain time of reaction, assume acetone formed is x μmol, water x μmol, IPA (20-x) μmol, and the amount of oxygen could be considered as constant.

Thus,

$$-282.9 \times 1000 = -8.314 \times 298.15 \times ln\frac{x^2}{(20-x)(4460)^{\frac{1}{2}}}$$

$$x > 19.99$$

That is, from the thermodynamic point of view, more than 99.9 % of IPA could be converted to acetone at the temperature of 25 °C.

The $\Delta G$ values were obtained from the Handbook "Thermochemical data of pure substances" by Ing. Ihsan Barin, 3rd edition.

Table S1 Physicochemical properties of the Au-based catalysts.

| Samples | Au (wt. %) [a] | Specific surface area ($m^2$ $g^{-1}$) [b] |
|---|---|---|
| $SrTiO_3$ | - | 1 |
| $SrTiO_3$-urea | - | 1 |
| Au/$SrTiO_3$ | 2.6 | 2 |
| Au/$SrTiO_3$-urea | 2.3 | 1 |
| $TiO_2$ | - | 7 |
| $TiO_2$-urea | - | 7 |
| Au/$TiO_2$ | 1.9 | 8 |
| Au/$TiO_2$-urea | 2.2 | 6 |

a, analyzed by ICP-OES method.

b, obtained by $N_2$ adsorption-desorption method through Brunauer-Emmett-Teller (BET) equation.

Table S2 Mass balances of the Au/$SrTiO_3$-urea catalyst in IPA dehydrogenation under dark condition.

| Time on stream (min) | IPA (μmol) | Acetone (μmol) | Mass balance (%) |
|---|---|---|---|
| 0 | 20.0 | 0.0 | 100.0 |
| 10 | 18.4 | 1.6 | 99.8 |
| 20 | 17.1 | 3.0 | 100.6 |
| 30 | 15.9 | 4.4 | 101.5 |
| 40 | 14.9 | 5.7 | 102.9 |
| 50 | 13.5 | 7.0 | 102.5 |
| 60 | 12.3 | 8.2 | 102.5 |

Table S3 Valence band and conduction band of the $SrTiO_3$ and $TiO_2$ related samples.

| Samples | Valence band (eV) | Conduction band (eV) |
|---|---|---|
| $SrTiO_3$ related samples | 3.0 | -0.2 |
| $TiO_2$ related samples | 2.9 | -0.4 |

The results were obtained from the UV-visible spectra in Fig. 3b and the Mott-Schottky plots in Fig. S13.

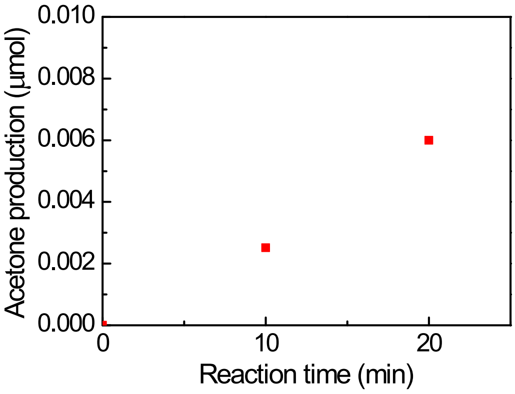

Fig. S1 Catalytic performance of the Au/$SrTiO_3$ catalyst prepared by photoreduction method in IPA dehydrogenation.

Reaction conditions: catalyst 0.15 g, initial IPA 20 μmol, room temperature (23 °C), without light irradiation.

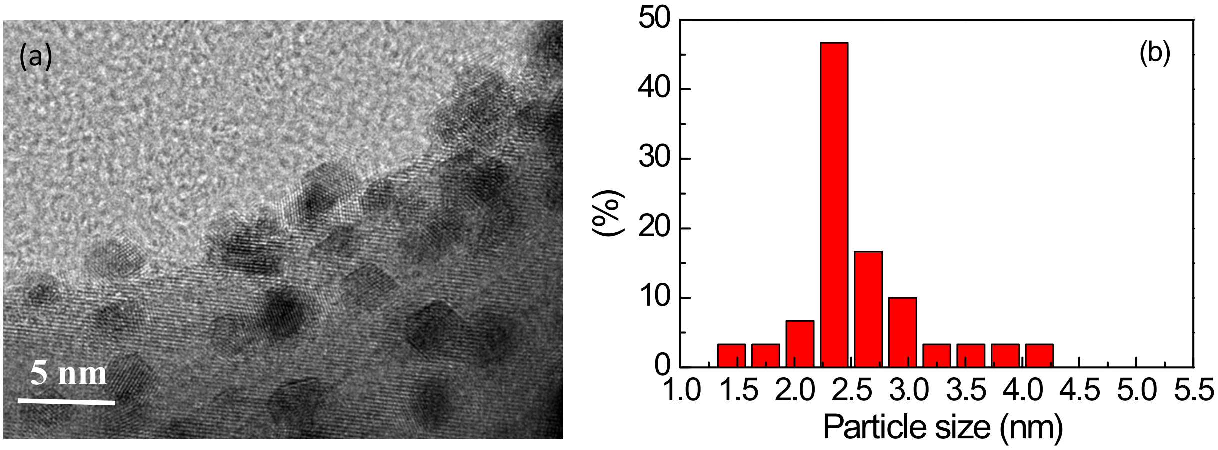

Fig. S2 (a) TEM image of Au/$SrTiO_3$ and (b) its Au particle size distribution.

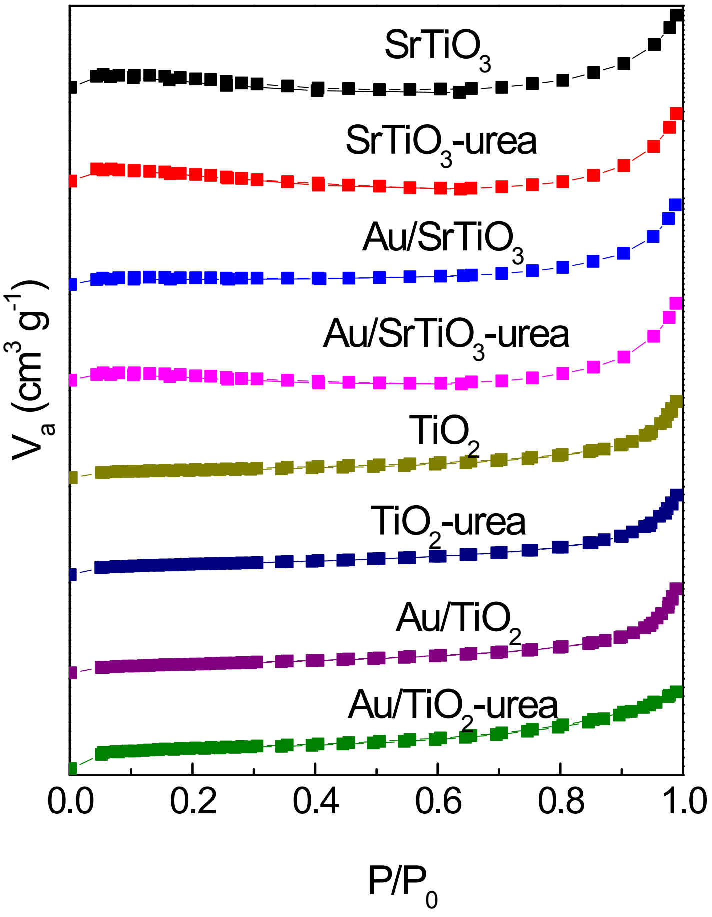

Fig. S3 Adsorption-desorption isotherms of the supports and catalysts.

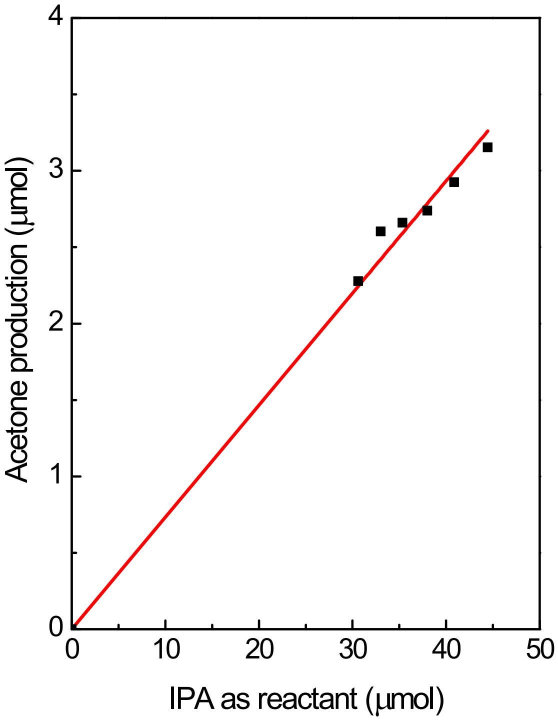

Fig. S4 Relationship between the amount of acetone production in 10 min and the initial IPA concentration at room temperature (23 $^{o}$C) over Au/SrTiO$_3$-urea without light irradiation.

Noticeably from Fig. S4, the amounts of acetone formation was nearly linearly related with the initial IPA concentration, that is, the reaction of IPA dehydrogenation was a first order reaction without light irradiation. Whereas for the solar light driven reactions, the reaction rate was generally considered to be associated with the amount of photon utilized, and then the amount of acetone generation was uncorrelated with the initial IPA concentration (zero order reaction) when it is a photocatalytic process [R1]. In this study, in order to discover the intrinsic performance and compare the catalytic performance of the catalysts, the initial IPA concentrations were normalized and all the other reaction conditions were kept as the same (20 μmol).

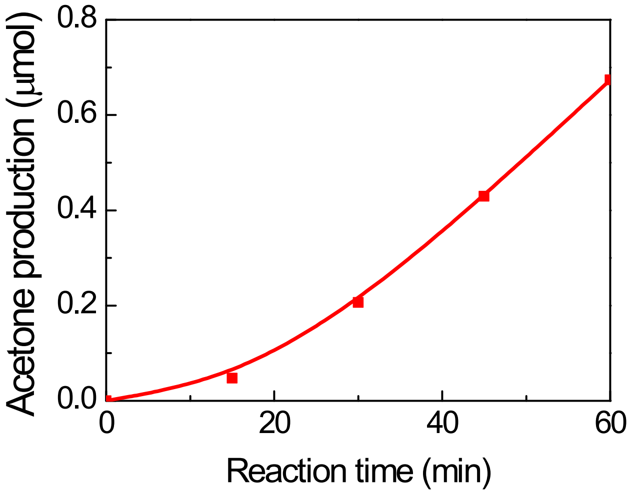

Fig. S5 Catalytic performance of Pt/$TiO_2$ catalyst in IPA dehydrogenation.

Reaction conditions: catalyst 0.15 g, initial IPA 20 μmol, room temperature (23 $^{o}$C), without light irradiation.

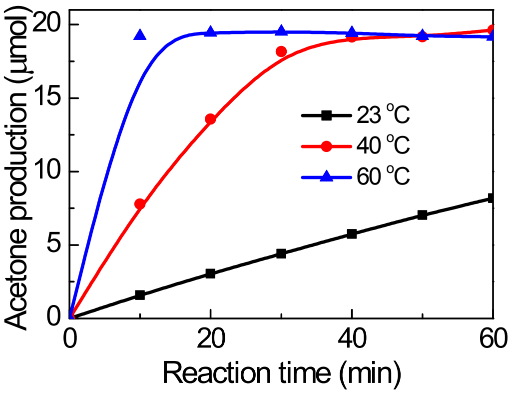

Fig. S6 Catalytic performance of Au/$SrTiO_3$-urea catalyst in IPA dehydrogenation at different reaction temperatures.

Reaction conditions: catalyst 0.15 g, initial IPA 20 μmol, without light irradiation.

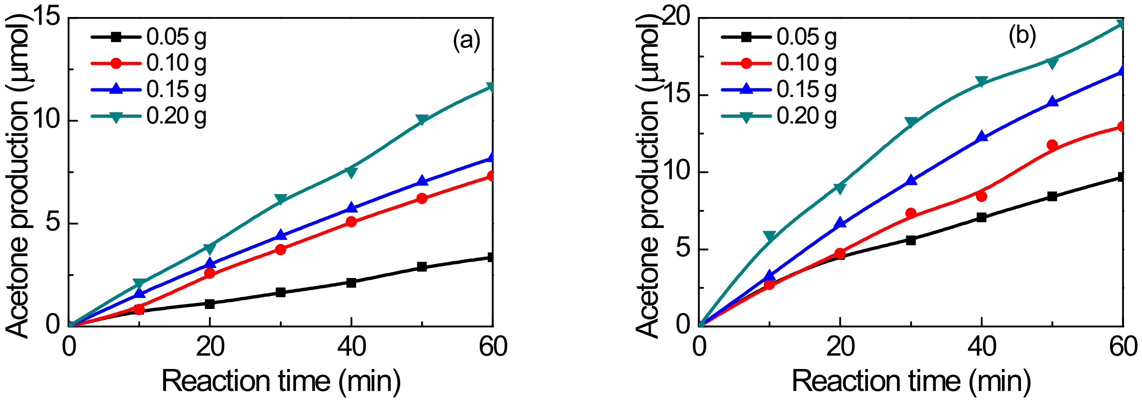

Fig. S7 Catalytic performance of Au/SrTiO$_3$-urea catalyst in IPA dehydrogenation with different catalyst dosage, (a) dark condition and (b) with visible light assistance.

Reaction conditions: initial IPA 20 μmol, room temperature (23 $^{o}$C).

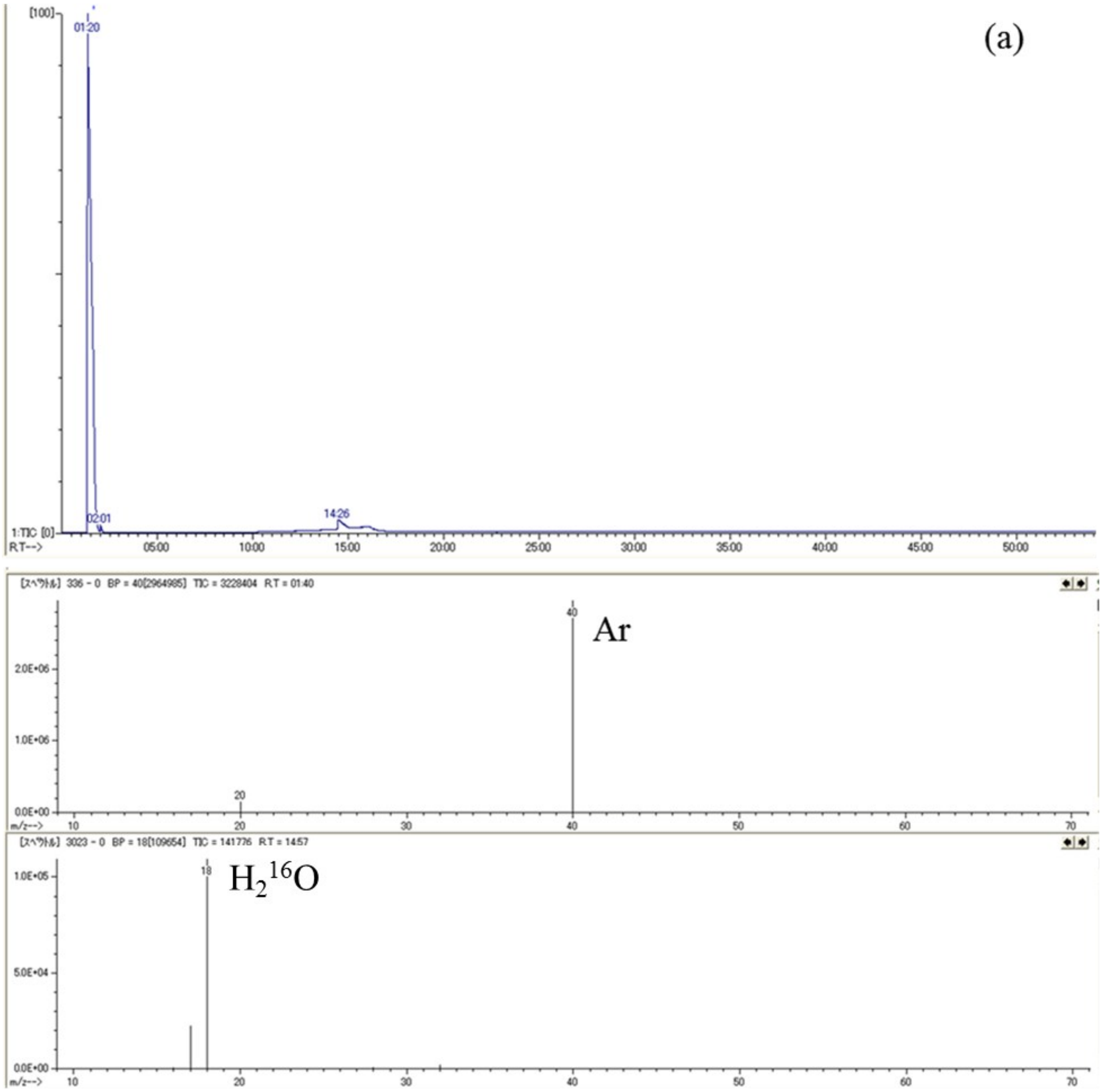
(a)
[100]
01:20
02:01
14:26
1:TIC [0]
RT-->
05:00
10:00
15:00
20:00
25:00
30:00
35:00
40:00
45:00
50:00
[スペクトル] 336 - 0 BP = 40[2964985] TIC = 3228404 R.T = 01:40
40
Ar
2.0E+06
1.0E+06
20
0.0E+00
m/z-->
10
20
30
40
50
60
70
[スペクトル] 3023 - 0 BP = 18[109654] TIC = 141776 R.T = 14:57
18
H2 16O
1.0E+05
5.0E+04
0.0E+00
m/z-->
10
20
30
40
50
60
70

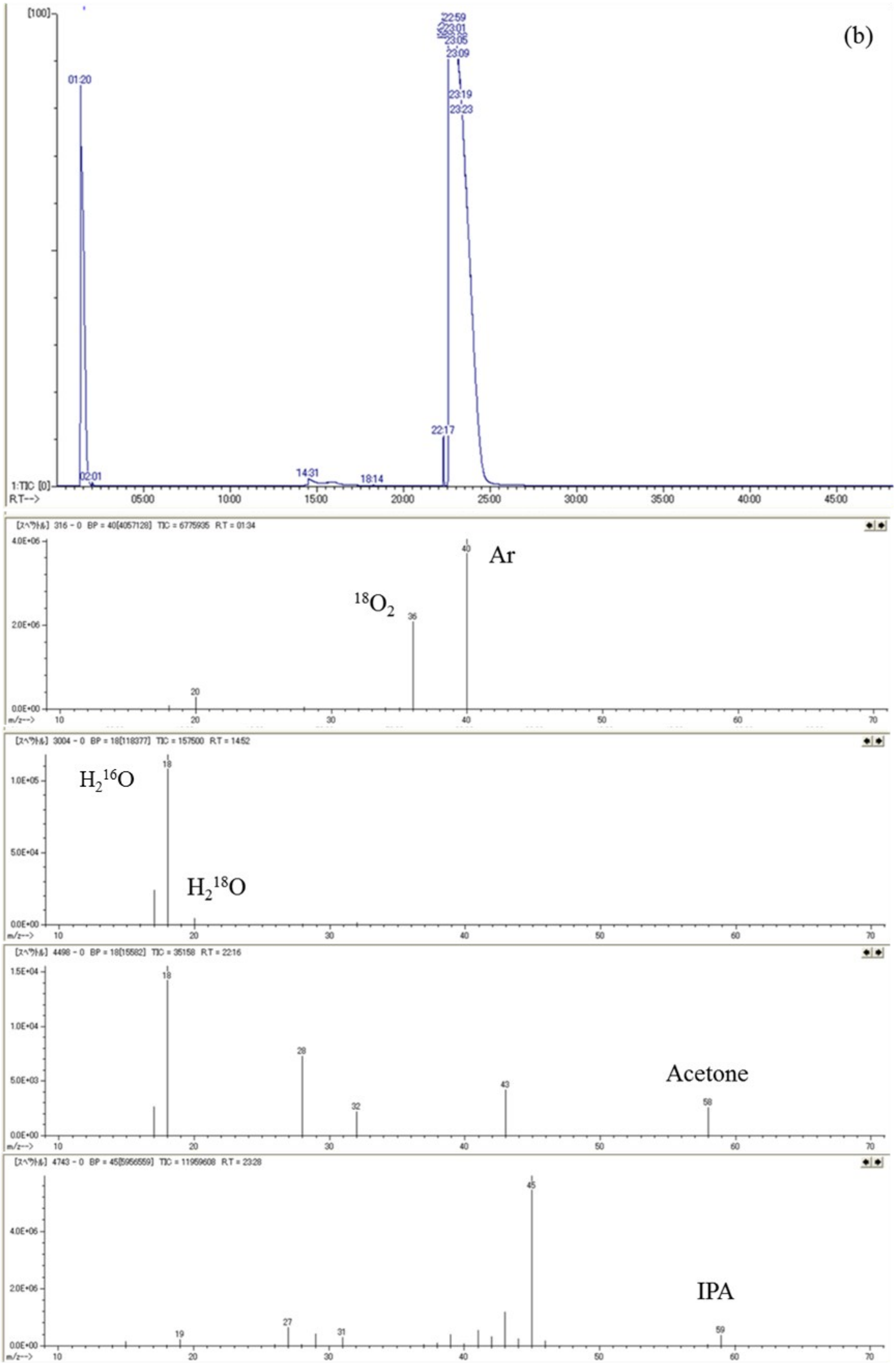

Fig. S8 $^{18}O_2$ isotope experiment over Au/$SrTiO_3$-urea catalyst.

Before isotope experiment, vacuum pressure was obtained by vacuuming the reactor for 5 days, and the peak appeared at about 15. 0 min was attributed to the water adsorbed on the columns of the GC. After isotope experiment, not only the intensity of $H_2{}^{16}O$ increased, the peak of $H_2{}^{18}O$ could also be observed.

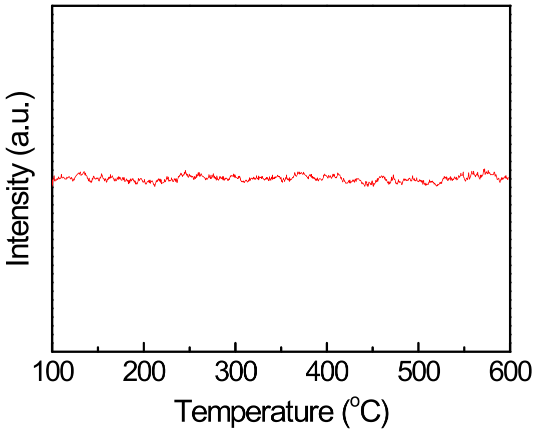

Fig. S9 $O_2$-TPD profile of Au/$SrTiO_3$-urea catalyst.

From the $O_2$-TPD profile, no peak could be observed, indicating that there was no peak attributed to urea decomposition (the decomposition temperature of urea is about 160 °C [R2]).

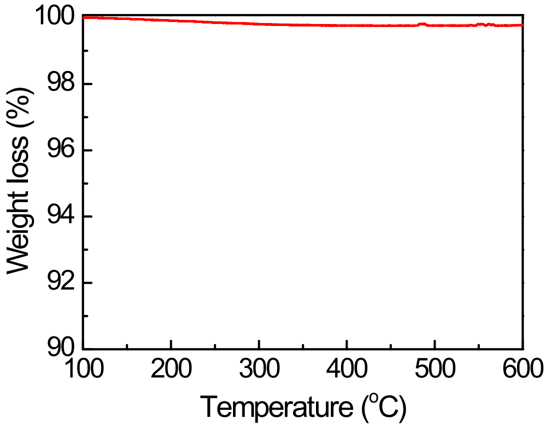

Fig. S10 TGA profile of Au/$SrTiO_3$-urea catalyst.

The TGA profile of Au/$SrTiO_3$-urea catalyst indicated that the weight loss in the temperature range of 100-600 °C was less than 0.2 %. Together with the $O_2$-TPD result in Fig. S9, it could be speculated that the residual urea in the washing process was nearly totally removed during the calcination process.

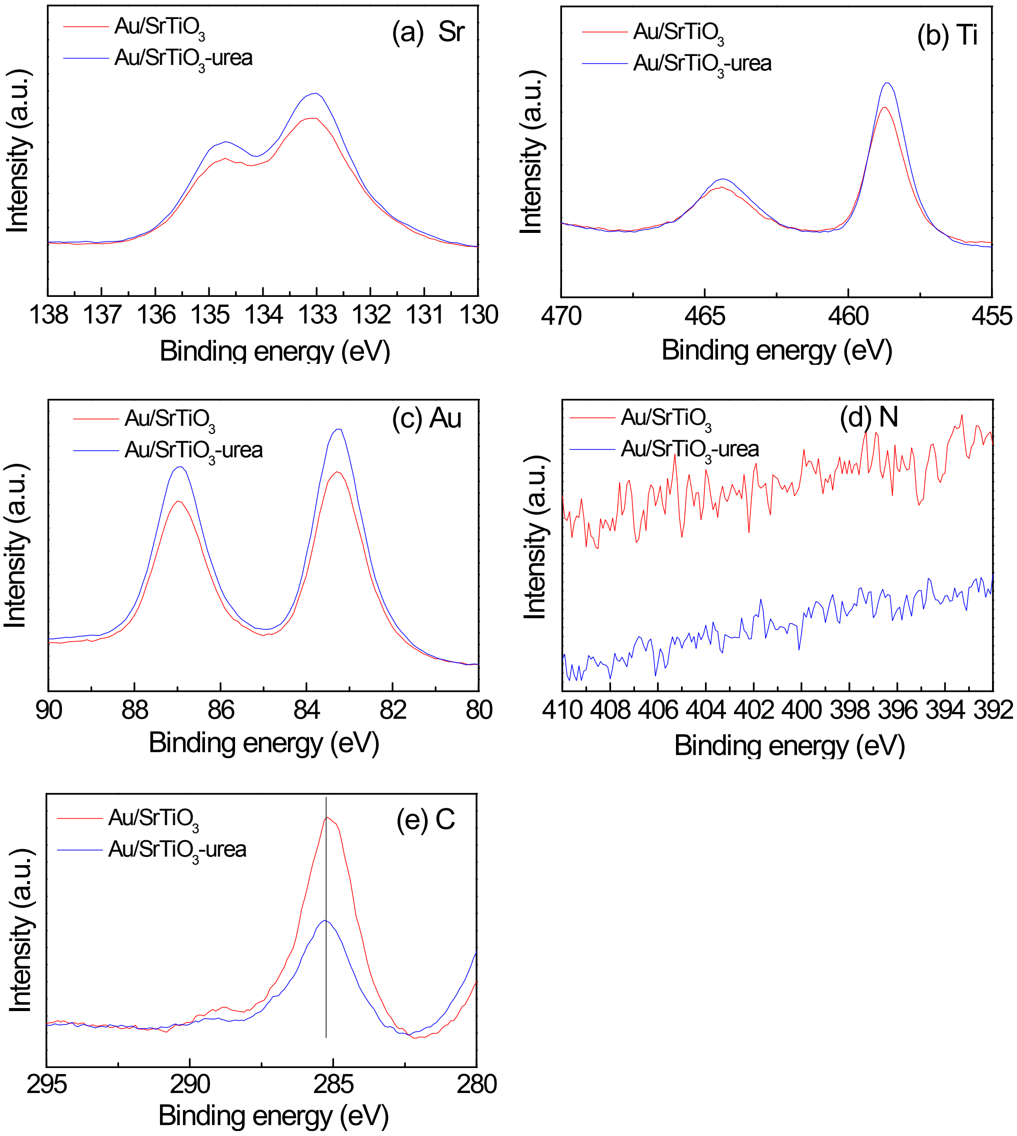

Fig. S11 XPS analysis of Au/SrTiO$_3$ and Au/SrTiO$_3$-urea.

From Fig. S11 it could be seen that the electronic structure and valence of Sr, Ti and Au were not greatly affected by the residual urea during catalyst preparation procedure. The reason was that the amount of N in the catalyst was quite small (it can be analyzed from the N XPS spectra). In spite that large peaks attributed to carbon was also detected from C XPS spectra, this did not guarantee that there were carbon residuals in the catalysts, since C XPS spectra could also be observed on carbon-free samples. The carbon detected was attributed to contaminated carbon.

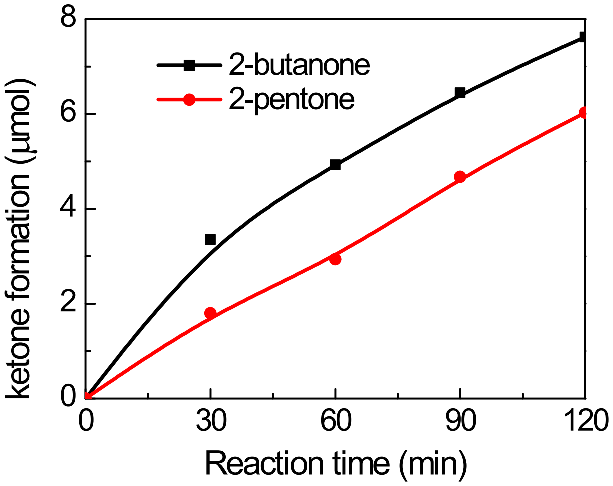

Fig. S12 Catalytic performance of the Au/SrTiO$_3$-urea catalyst in 2-butanol and 2-pentanol dehydrogenation.

Reaction conditions: catalyst 0.15 g, initial 2-butanol/2-pentanol 20 μmol, room temperature (23 °C), without light irradiation.

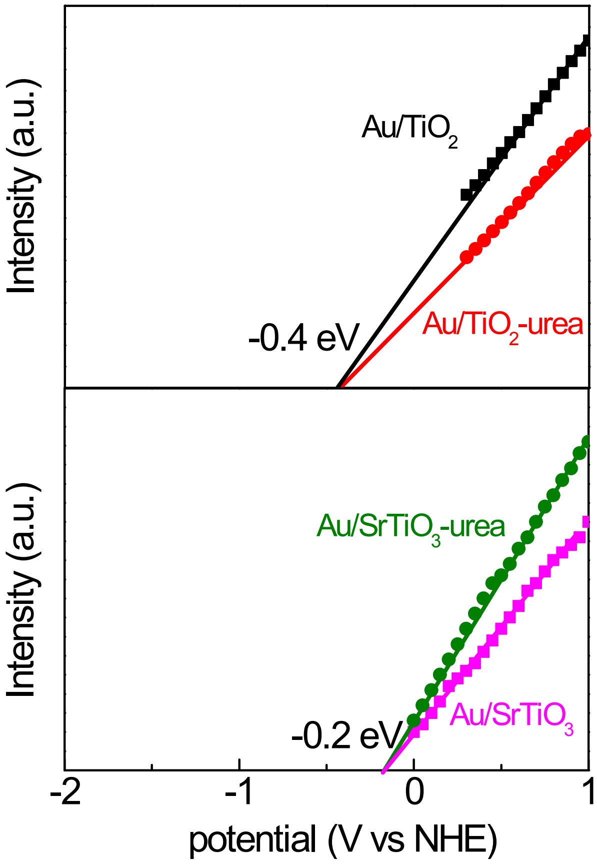

Fig. S13 Mott-Schottky plots of the Au-based catalysts.

Mott-Schottky plots were employed to characterize the conduction band of the Au-based catalysts, it could be seen from Fig. S13 that the conduction band of Au/$TiO_2$ and Au/$TiO_2$-urea was -0.4 eV, and the conduction band of Au/$SrTiO_3$ and Au/$SrTiO_3$-urea was -0.2 eV. Together with the band gap analysis in Fig. 3b, the valence band of the catalysts could be obtained and listed in Table S3.

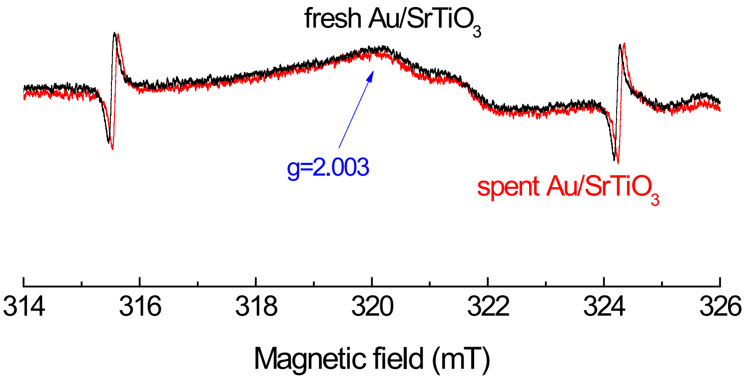

Fig. S14 *In-situ* ESR profiles of Au/SrTiO$_3$-urea in IPA dehydrogenation.

The signal at g=2.003 was assigned to the oxygen vacancies by O$^-$ anion radicals [R3]. As it is proposed in the mechanism study part of Au/SrTiO$_3$-urea in IPA dehydrogenation without light irradiation, with the extraction of the lattice oxygen in generating the byproduct water, oxygen vacancy would be formed. However, the *in-situ* ESR profile indicated that the intensity of the peak attributed to oxygen vacancy did not change as the reaction occurred. Together with the results shown in Fig. 2b and Fig. S8, it could be proposed that the oxygen vacancies were soon occupied with atmospheric oxygen (Scheme 1).

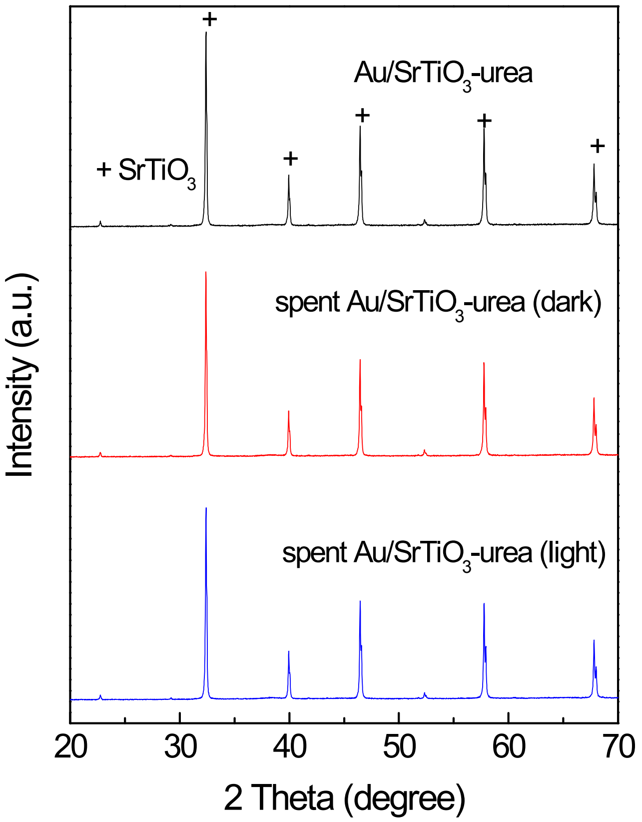

Fig. S15 XRD patterns of the fresh and spent Au/$SrTiO_3$-urea catalysts.

The XRD patterns of the fresh Au/$SrTiO_3$-urea catalyst exhibited no diffraction peaks attributed to Au species, indicating the Au particles were very small. The XRD patterns before and after reaction revealed that the structure of the catalysts did not change during the reaction of IPA dehydrogenation with/without visible light irradiation.

## References

[R1] S. Ouyang and J. Ye, β-$AgAl_{1-x}Ga_xO_2$ solid-solution photocatalysts: continuous modulation of electronic structure toward high-performance visible-light photoactivity, J. Am. Chem. Soc., 133 (2011) 7757–7763.

[R2] R. Zanella, S. Giorgio, C. Shin, C. R. Henry and C. Louis, Characterization and reactivity in CO oxidation of gold nanoparticles supported on $TiO_2$ prepared by deposition-precipitation with NaOH and urea, J. Catal., 222 (2004) 357–367.

[R3] M. Sterrer, E. Fischbach, T. Risse and H. J. Freund, Geometric characterization of a singly charged oxygen vacancy on a single-crystalline MgO(001) film by electron paramagnetic resonance spectroscopy, Phys. Rev. Lett., 94 (2005) 186101.